THEORETICAL ANALYSIS FOR FLOW CONDENSATION HEAT AND MASS TRANSFER OF ZEOTROPIC MIXTURES IN A HORIZONTAL SMOOTH TUBE

Qin Wang[1], Qinglu Song[1,2,*], Chuantong Zhang[1], Bin Sun[3], Sai Zhou[1], Dechang Wang[1,**]

[1]College of Mechanical and Electrical Engineering, Qingdao University, Qingdao 266071, China

[2]School of Energy and Environment, City University of Hong Kong, Hong Kong, China

[3]Department of Refrigeration System R&D, Hisense R&D Center, Qingdao, China

[*]Corresponding author: sql@qdu.edu.cn

**Corresponding author: wdechang@163.com

As the increasingly serious impact of CFCs and HFCs on the environment, research on zeotropic mixtures plays an indispensable role in many industries. Especially, the study of zeotropic mixtures is essential for optimizing Liquefied Natural Gas system design. As primary constituents of natural gas, methane (R50) and ethane (R170) are equally vital in mixed-refrigerant Joule-Thomson cycles. This work experimentally examines flow condensation heat transfer for R50/R170 blends in horizontal smooth tubes across wide-ranging conditions. A non-equilibrium film theory-based analytical model was proposed to examine heat and mass transfer during binary zeotropic mixture condensation, incorporating vapor-liquid interfacial mass transfer resistances. Rigorous examination quantified impacts of mass flux, saturation pressure, heat flux, and vapor quality on temperature and concentration gradients. The results revealed substantial heat transfer degradation from temperature/mass fraction gradients, exhibiting strong dependency on volatile component concentration and mixture vapor quality. Model predictions demonstrated good agreement with measured condensation heat transfer coefficients for binary refrigerants.

Key words: *Zeotropic mixture, Methane and ethane, Heat and mass transfer, Nonequilibrium film theory*

1. Introduction

Liquefied natural gas (LNG) facilitates global trade due to its significantly higher density in liquid form. The design and manufacturing of LNG facilities critically depend on core thermodynamic properties and experimental data. Within these, heat transfer characteristics of condensation are particularly vital for LNG liquefaction, storage and conveyance. Methane (R50) and ethane (R170), the primary constituents in natural gas, have been experimentally studied in published literature. Maråk [1] conducted an experimental study on the condensation heat transfer coefficients of R50 and the R50/R170 mixture in a circular tube with an inner diameter of 1 mm. The results show that the condensation heat transfer coefficients of both R50 and the R50/R170 mixture increase with the increase in mass flux and vapor quality, and decrease with the increase in saturation pressure. However, when Zhuang et al. [2, 3] measured the condensation heat transfer coefficients of R50, R170, and the R50/R170 mixture in a horizontal circular tube, they found that due to the mixing effect, the condensation heat transfer coefficient of the R50/R170 mixture does not increase monotonically with the increase in vapor quality.

Moreover, R50 and R170 also serve as essential constituents in mixtures for mixed-refrigerant Joule-Thomson (MRJT) cycle [4-6]. MRJT refrigeration cycle is predominant liquefaction technology in the LNG industry [7]. Due to the characteristics of high efficiency, low cost and high reliability of the MRJT refrigeration technology, it has a wide application in temperature range from liquid nitrogen conditions to conventional single-stage vapor-compression refrigeration limits (80-230 K). Tzabar [8] experimentally investigated the performance of Joule-Thomson cryocoolers using two binary mixed refrigerants: N_2/R170 and N_2/R290. The results showed that the N_2/R170 mixed refrigerant exhibited excellent adaptability across various cooling temperature requirements. Moreover, when the molar concentration of N_2 in the mixed refrigerant exceeded 55%, N_2/R170 demonstrated better refrigeration stability and efficiency under operating conditions where the target cooling temperature was above 100 K. Wang et al. [9] employed a seven-component mixed refrigerant at 1.8 MPa (high-pressure) and 0.3 MPa (low-pressure), among which the temperature zone of R50 is 125-150 K and R170 is180-214 K. In addition, the single-stage MRJT cooler operating at 100-200 K was analyzed in their later research [10]. Optimization of mixed refrigerants was conducted at distinct operating pressures. Zou et al. [11] employed the MRJT technology with R1150/R600 as working fluids, achieving 203.15 K Refrigeration in sub-ambient freezers (298.15 K environment). In addition, for zeotropic mixture, it can provide better temperature matching with variable temperatures of heat source and sink, hence decreasing irreversible losses in heat transfer process. Therefore, R50/R170 transfer characteristic of flow condensation is essential to MRJT refrigerator design and optimization.

It is difficult to obtain temperature and concentration gradients of zeotropic mixtures experimentally during condensation process. Over the past few decades, many theoretical investigations elucidate condensation mechanisms of mixtures in heat and mass transfer Initial formulation of the non-equilibrium model traces to Colburn and Drew [12]. Since the process of zeotropic mixture condensation is accompanied by the decrease of two-phase temperature, it is proposed that total condensation heat is composed of latent heat, sensible heat of condensate and vapor phase. After that, in order to facilitate the solution, Price and Bell [13] optimized and reconstructed the equation. This model assumes local thermodynamic equilibrium at the interface of two phases. Non-equilibrium refers to the bulk fluid states, while interfacial concentration and temperature remain equilibrated.

The non-equilibrium theory has been adopted in many studies. The non-equilibrium model for flow condensation was employed by Jin et al. [14] to forecast heat transfer performance of R134a/R123. This investigation incorporated vapor-liquid mass transfer resistances and applied the high-flux correction factor for mass transfer coefficient evaluation. Results revealed negligible influence of this factor on condensation heat transfer performance. Extending prior frameworks, Wang et al. [15-17] established a non-equilibrium film transfer model with both two phase resistance consideration. The resistances in heat and mass transfer were deeply discussed. They indicated that heat transfer degradation coefficient increases with the reduction of mass fluxes. Deng et al. [18] employed higher-order finite elements to simulate zeotropic mixture characteristics of heat and mass transfer.

Their model accounts for vapor-phase resistances to both heat and mass transfer. Their results demonstrated an inverse relationship between mass flux and heat transfer degradation coefficient. The vapor-liquid interface exhibits enriched more volatile component concentration in comparison with bulk vapor, and interfacial enrichment of the more volatile component diminishes with decreasing vapor quality and rising mass flux relative to bulk vapor composition. However, the calculated heat transfer coefficient versus vapor quality exhibits anomalous, especially a sharp increase at high vapor quality zone. Zhang et al. [19] established a theoretical model addressing zeotropic mixture characteristics of flow condensation. Surface tension was limited to considering the Marangoni effect of zeotropic mixtures. The result indicated that vapor-phase transfer resistances in heat and mass diminish with increasing mass flux, saturation pressure, and tube diameter. Recently, Wu et al. [20] formulated a non-equilibrium model considering concentration gradient in both two phases. The model revealed that vapor-phase boundary layer gradients in concentration and temperature reduce the driving temperature difference by 20–30%, indicating a significant heat transfer degradation resulted from the gradient effect. Yan et al. [21] formulated a simplified non-equilibrium model by introducing several empirical formulas. The boiling point disparity between the two components was incorporated to characterize the concentration gradient and mass transfer. Furthermore, Yan et al. [22] extended the model to ternary mixtures, achieving satisfactory results with 90.2% of data points showing absolute deviations less than 30%.

For the design and optimization of heat exchangers in the MRJT cycle, research on the heat and mass transfer characteristics of zeotropic mixtures is of crucial importance. Although previous studies have conducted extensive work on heat transfer models, there remains a gap in the accurate quantification of their non-equilibrium characteristics. In this study, a theoretical heat transfer model for binary mixture in horizontal tube flow condensation is developed. The 'real interface temperature' and 'real interface concentration' can be calculated using this model. Subsequently, the temperature and concentration gradients during the zeotropic mixtures flow condensation process can be quantified. The model is verified according to our experimental data of methane/ethane [23]. A parametric investigation on the effects of composition, mass flux, saturation pressure and heat flux were carried out.

2. Physical and mathematical model

2.1 Physical model

The present physical model represents condensation of mixtures in annular flow within horizontal pipes. As shown in Fig. 1, both the resistances of heat and mass transfer in the two-phases are contained. All the mixture thermophysical properties used in this study are retrieved from NIST REFPROP 9.1 [24].

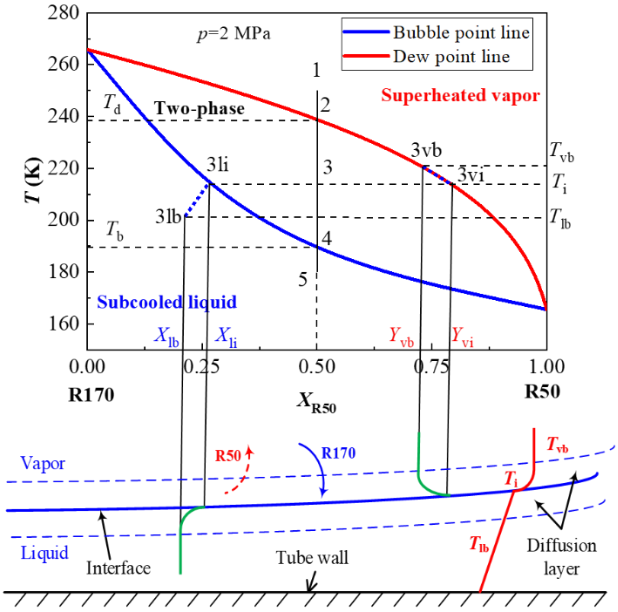

Fig. 1. Schematic view of the flow condensation process of R50/R170 mixture.

The model incorporates the following assumptions:

(1) Local phase equilibrium exists exclusively at the two-phase interface;

(2) Non-equilibrium exists within interfacial boundary layers, where mass transfer occurs, and vapor is saturated and liquid is subcooled;

(3) Heat transfer coefficients of liquid film are determined by pure-fluid condensation correlations [2];

(4) Circumferentially uniform annular flow maintains constant liquid film thickness;

(5) Neglecting the effect of the pressure drop.

2.2 Mathematical model

2.2.1 Condensation heat transfer coefficient

Based on the thermal equilibrium in working fluid, the heat flux of tube wall are formulated by Eq. (1).

$$q=h\left(T_{\mathrm{vb}}-T_{\mathrm{w}}\right)=h_{\mathrm{l}}\left(T_{\mathrm{i}}-T_{\mathrm{w}}\right) \tag{1}$$

Wherein, q is local heat flux, W m^{-2}; T_{vb} is vapor bulk temperature and is computed from enthalpy and composition data, K; T_{w} is the local temperature of inner-wall, K; h_{l} is the liquid film heat transfer coefficient, W m^{-2} K^{-1}; T_{i} is local saturation temperature corresponding to local pressure, K. The local condensation heat transfer coefficient can be expressed as follows:

$$h=\frac{T_{\mathrm{i}}-T_{\mathrm{w}}}{T_{\mathrm{vb}}-T_{\mathrm{w}}}h_{\mathrm{l}} \tag{2}$$

2.2.2 Mass transfer

The mass condensation flux of the total process (m_{t}) and the mass condensation flux of the more volatile component (m_1) are computed by the mass conservation in vapor-side:

$$m_{\mathrm{t}}=-\frac{GD_{\mathrm{w}}^{2}}{4D_{\mathrm{v}}}\frac{\mathrm{d}x}{\mathrm{d}z} \tag{3}$$

$$m_{\mathrm{l}}=-\frac{GD_{\mathrm{w}}^{2}}{4D_{\mathrm{v}}}\frac{\mathrm{d}\left(xY_{\mathrm{vb}}\right)}{\mathrm{d}z} \tag{4}$$

where, G is the mass flux, kg m^{-2} s^{-1}; D_{w} is inner diameter of the tube wall, m; D_{v} is the vapor phase hydraulic diameter, m; Y is the vapor concentration of more volatile component; x is the vapor quality; z is the position of the condensation section.

More volatile component condensation flux constitutes diffusive and convective components, computable through vapor/liquid-side analysis:

$$m_{\mathrm{l}}=m_{\mathrm{t}}Y_{\mathrm{vi}}-k_{\mathrm{v}}\rho_{\mathrm{v}}\left(Y_{\mathrm{vi}}-Y_{\mathrm{vb}}\right) \tag{5}$$

$$m_{\mathrm{l}}=m_{\mathrm{t}}X_{\mathrm{vi}}+k_{\mathrm{l}}\rho_{\mathrm{l}}\left(X_{\mathrm{li}}-X_{\mathrm{lb}}\right) \tag{6}$$

where, X is the vapor concentration of more volatile component; k_{v} and k_{l} are the vapor-phase convective mass transfer coefficient and liquid-phase convective mass transfer coefficient, respectively, kg m^{-2} s^{-1}, and it can be calculated by Koyama et al. [25] and Lamourelle et al. [26] correlation, respectively, as follows:

$$k_{\mathrm{v}}=\frac{Sh_{\mathrm{v}}\rho_{\mathrm{v}}J_{\mathrm{v}}}{D_{\mathrm{v}}}=0.023Re_{\mathrm{v}}^{0.8}Sc_{\mathrm{v}}^{1/3}\frac{\rho_{\mathrm{v}}J_{\mathrm{v}}}{D_{\mathrm{v}}} \tag{7}$$

$$k_{\mathrm{v}}=\frac{Sh_{\mathrm{l}}\rho_{\mathrm{l}}J_{\mathrm{l}}}{D_{\mathrm{l}}}=\left(1.76\times10^{-5}\right)Re_{\mathrm{l}}^{1.506}Sc_{\mathrm{l}}^{0.5}\frac{\rho_{\mathrm{l}}J_{\mathrm{l}}}{D_{\mathrm{l}}} \tag{8}$$

where, J_{v} and J_{l} represent the diffusion coefficients of the vapor phase and liquid phase, respectively, m^{2} s^{-1}, which can be obtained Hayduk and Minhas and Chapman Enskog [27] correlation. Re is the Reynolds number; Sc is the Schmidt number, Sc_{v} and Sc_{l} can be calculated by:

$$Sc_{\mathrm{v}}=\frac{\mu_{\mathrm{v}}}{\rho_{\mathrm{v}}J_{\mathrm{v}}} \tag{9}$$

$$Sc_{\mathrm{l}}=\frac{\mu_{\mathrm{l}}}{\rho_{\mathrm{l}}J_{\mathrm{l}}} \tag{10}$$

2.3 Solution procedure

Considering a control volume spanning axial positions z to $z+\Delta z$ within the condenser, numerical solutions are obtained for the derived thermal and mass transport equations. This solution requires prior specification of two boundary conditions: (1) inner-wall axial temperature profile, and (2) saturated vapor mixture conditions at the refrigerant inlet. The computational algorithm, initialized with saturated vapor at the inlet, executes the following sequence:

(1) Define the control volume length, and get the inlet thermodynamic properties.
(2) Outlet vapor quality is determined through refrigerant energy balance.
(3) Calculate the total mass condensation flux and the mass condensation flux of the more volatile component from Eqs. (3) and (4).
(4) Evaluate vapor-phase dimensionless groups (Re, Pr, Sc, Nu, Sh) and subsequently determine convective heat/mass transfer coefficients.
(5) Obtain the Y_{vi} and X_{li} from Eqs. (5) and (6).

(6) Calculate T_i from thermodynamic state equations based on interface concentration.

(7) Determine the heat transfer coefficient of liquid-film utilizing pure fluid heat transfer correlations with mixture thermophysical properties.

(8) Eqs. (1) and (2) are utilized to calculate the wall temperature and heat transfer coefficient.

(9) Assign outlet conditions as inlet states for the subsequent control volume.

(10) Iterate until vapor quality $x \leq 0$.

3. Results and discussion

Fig. 2 (a) depicts the variation of the concentration of R50 under different vapor quality conditions at both two phases. All the mass fractions of R50 increase as the condensation process. Moreover, both the interface values of two phases are greater than the relative bulk values. During the condensation process, R170 undergoes preferential phase change. This will lead to accumulation of R50 within the interfacial diffusion layer, elevating its local concentration. Back diffusion of R50 occurs from the interface toward the vapor bulk, where concentrations are lower. A comparable concentration gradient forms within the liquid film. Besides, as noted in this figure, the concentration gradient in liquid-side dominates the lower vapor quality region, and the vapor-side concentration gradient in dominates the higher vapor quality region. The main reason is that, at low vapor quality, the liquid phase fraction is large and the liquid film is thick, so the liquid side mass-transfer resistance dominates and the liquid side concentration difference is larger, making the liquid concentration gradient more sensitive to vapor quality. At high vapor quality, the vapor-phase mass transfer resistance dominates the condensation process. To maintain the condensation flux, it is necessary to increase the vapor-phase mass transfer driving force, i.e. the vapor-phase concentration difference. Fig. 2 (b) presents axial temperature distributions for bulk vapor, two-phases interface, and condenser wall. Along the condenser length, all temperatures decrease monotonically. Due to resistance in mass transfer, the interfacial temperature consistently remains below the bulk vapor temperature. Nevertheless, this difference progressively disappears as condensation approaches completion.

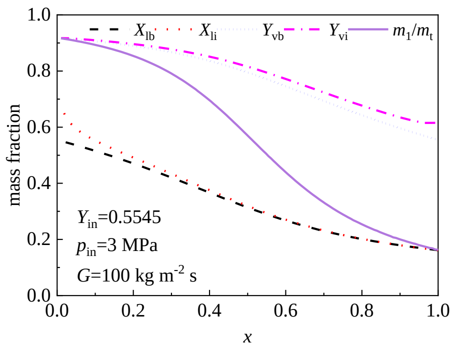

Fig. 2 (a) Mass fraction variation with vapor quality.

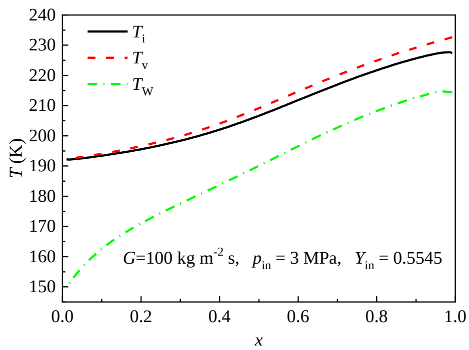

Fig. 2 (b) Temperature variation with vapor quality.

3.1 Effect of mass flux

The effects of mass flux on the concentration gradients at both phases are depicted in Fig. 3. It can be clearly noted that the vapor-side concentration gradient (Y_{vi}-Y_{vb}) reduces with condensation process (the decrease of vapor quality), and almost disappears as condensation approaches completion. While, the liquid-side concentration gradient (X_{li}-X_{lb}) increases with the condensation process. It can also be observed that both the two-phase concentration gradients reduction with the mass flux, which is resulted from the well-mixed mixture of both two phases at the higher mass flux. A higher mass flux can enhance turbulence of fluid, thereby diminishing the two-phase concentration gradients. As can be seen from Fig. 3, in the low vapor-quality region, the liquid-phase concentration difference decreases significantly as the mass flux increases; in the high vapor-quality region, the vapor-phase concentration difference, in turn, decreases significantly with increasing mass flux. This is because in low vapor-quality region, the liquid phase accounts for a higher proportion, making the liquid-phase concentration difference more sensitive to the mass flux. Conversely, in high vapor-quality region, the vapor phase accounts for a higher proportion and vapor-phase mass transfer resistance dominates, and the vapor-phase concentration difference is more sensitive to changes in the mass flux.

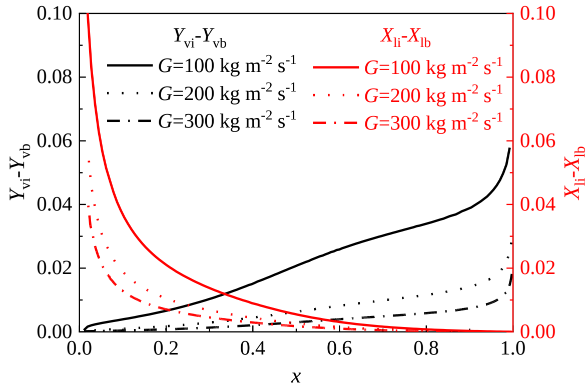

Fig. 3. Mass fraction variation with vapor quality at different mass flux.

As can be noted in Fig. 4 (a), the temperature difference across the bulk vapor to vapor interface during phase change (T_v−T_i) shows an upward trend with increasing vapor quality while demonstrating a downward trend with rising mass flux, which means that a greater temperature gradient occurs at the higher vapor quality regions. It can be attributed to the turbulence of the fluid at low mass flux is lower, which results in a slower heat transfer rate. Therefore, it is difficult for the heat to be migrate from the bulk vapor toward vapor-liquid interface, and then resulting in a greater (T_v−T_i). Fig. 4 (b) depicts the variation of heat transfer degradation coefficient (T_i - T_w)/(T_v - T_w) with vapor quality under varying mass flux conditions. The heat transfer degradation factor decreases with increasing vapor quality, attributable to the enhancement of mass transfer effects. The heat transfer degradation coefficient reaches its peak at the condenser inlet, while approaching 1 at the outlet, illustrating a very small degradation of heat transfer. Similar trends as mass flux varies were also observed for the heat transfer degradation factor. In addition, heat transfer degradation factor increases with the mass flux as shown in Fig. 4 (b). For zeotropic mixture, the heat transfer degradation is mainly resulted from temperature glide and resistance in mass transfer [28-30]. At high mass flux, the turbulence degree is greater, leading to a smaller concentration gradient of R50, and then mass transfer resistance decreases. The results is consistent with that of Wang et al. [31]. They reported that the degree of heat transfer degradation is alleviated by increasing mass fluxes.

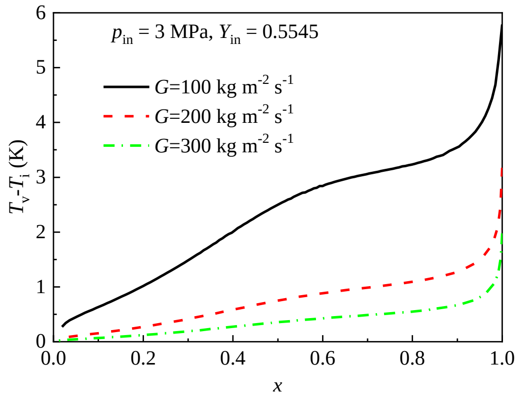

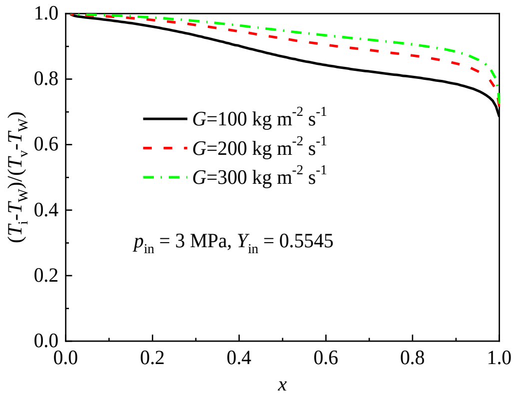

Fig. 4 (a) Temperature gradient variation with vapor quality at different mass flux.

Fig. 4 (b) Heat transfer degradation factor variation with vapor quality at different mass flux.

3.2 Effect of saturation pressure

As depicted in Fig. 5 (a), the vapor-side concentration gradient (Y_{vi}-Y_{vb}) declines as condensation proceeds (the reduction of vapor quality), and the liquid-side concentration gradient (X_{li}-X_{lb}) increases with the condensation process. While, the impact of saturation pressure on vapor-side concentration gradients is more complicated. The vapor-side concentration gradients intensify at lower pressures when x>0.5, but diminish when x < 0.5. This is mainly related to the variation of the vapor-side interfacial equilibrium concentration and the mass transfer coefficient. Changes in the saturation pressure alter the interfacial temperature, thereby affecting the vapor-side interfacial equilibrium concentration, and also modify the vapor-side mass-transfer coefficient through changes in the diffusion coefficient and liquid film characteristics. In addition, due to the thermophysical properties and mass transfer coefficient of the liquid phase are less affected by the variation of saturation pressure, the concentration difference in the liquid phase exhibits insignificant variation.

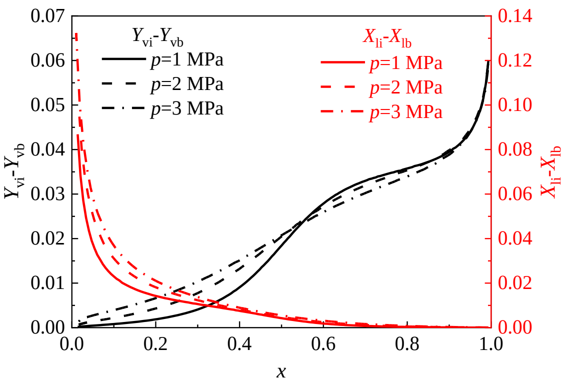

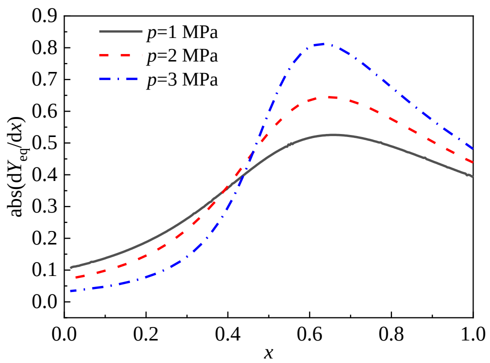

Fig. 5 (a) Mass fraction variation with vapor quality at different saturation pressure.

Fig. 5 (b) Equilibrium vapor composition gradient against quality at different pressures.

Fig. 5 (b) presents the equilibrium vapor composition gradient as a function of quality under varying pressures. It can be found that absolute value of vapor composition gradient against quality increases first and then reduces with the vapor quality, indicating that resistance in mass transfer is greater at the high vapor quality zone. Moreover, the absolute value of vapor composition gradient against quality is larger at higher pressure when x > 0.5 and the reversal in this trend emerges when x <

0.5. Different variation trends of vapor composition gradient lead to different influences of saturation pressure.

3.3 Effect of heat flux

The effects of mass flux on the concentration gradients at both phases as illustrated in Fig. 6 (a). It can be clearly observed that the vapor-side concentration gradient decreases with the decrease of vapor quality, and the liquid-side concentration gradient has the opposite trend. This is because, as the heat flux increases, the overall condensation rate rises, and the condensation of R170 at the interface intensifies, leading to an enrichment of the more volatile component R50 near the interface. As a result, both the vapor-side and liquid-side interfacial concentrations increase, thereby markedly enlarging the concentration gradients in both phases. Different from the influence of mass flux, a larger heat flux can induce higher concentration gradients in both phases. It is worth noting that in the low vapor-quality region, the liquid-phase mass transfer resistance dominates, which makes the response of the liquid-phase concentration difference to heat flux more significant. However, in the high vapor-quality region, the vapor-phase mass transfer resistance dominates, leading to a significant increase in the vapor-phase concentration difference. Although the concentration gradients are significantly influenced by the heat flux, these influences are not transmitted to the heat transfer ability. As depicted in Fig. 6 (b), the heat transfer degradation factor exhibits minimal dependency on heat flux, which results from the fact that a higher heat flux can increase the heat transfer driving force during the phase change process, thereby mitigating mass transfer resistance effects and stabilizing the heat transfer degradation factor.

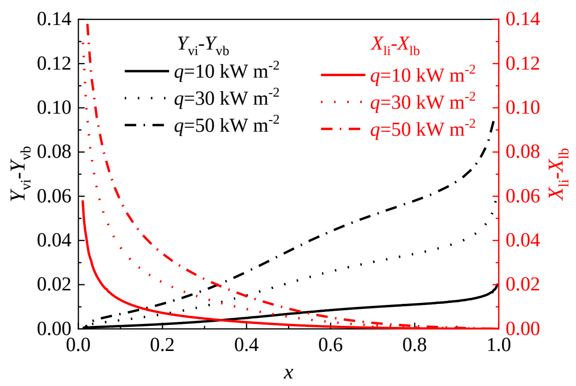

Fig. 6 (a) Mass fraction variation with vapor quality at different heat flux.

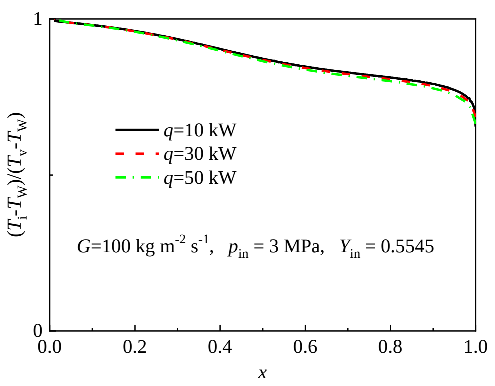

Fig. 6 (b) Heat transfer degradation factor variation with vapor quality at different heat flux.

3.4 Compared with the experimental data

The model undergoes validation through comparative analysis of measured and predicted heat transfer coefficients. Experimental versus computed condensation heat transfer coefficients are compared with vapor quality in Fig. 7(a). The calculated line can well character the variation tendency of experimental condensation heat transfer coefficients at different experimental conditions. What's more, the absolute relative deviation (ARD) and the mean absolute relative deviation (MARD) were utilized to evaluate the predictive ability of the present model. As evidenced in Fig. 7 (b), the model achieves accurate predictions, exhibiting an ARD of -0.14% and MARD of 11.47% versus experimental data.

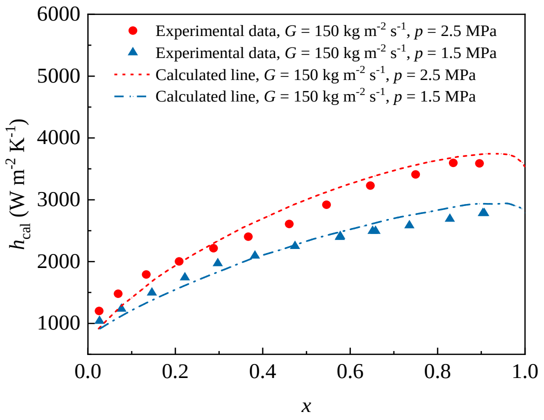

Fig. 7 (a) Compared with the flow condensation heat transfer experimental data.

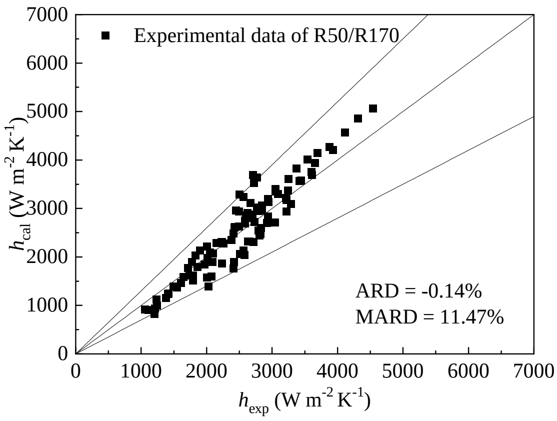

Fig. 7 (b) Comparison between the predicted and experimental results.

4. Conclusions

In this paper, a theoretical analysis of R50/R170 flow condensation using non-equilibrium film theory was conducted, incorporating both two phase mass transfer mechanisms. Temperature and concentration gradient dependencies on mass flux, saturation pressure, heat flux, and vapor quality underwent systematic investigation. The core conclusions are emerged as listed.

(1) The higher vapor quality region was dominated by vapor-side concentration gradient, while the lower vapor quality region was dominated by liquid-side concentration gradient.

(2) High mass flux reduces both-phase resistances in heat and mass transfer. In the low vapor-quality region, the liquid-phase concentration difference decreases significantly as the mass flux increases; in the high vapor-quality region, the vapor-phase concentration difference, in turn, decreases significantly with the increase in mass flux.

(3) Both two-phase concentration gradients increase with heat flux, while it has a little impact on the flow condensation heat transfer performance. In the low vapor-quality region, the liquid-phase concentration difference increases significantly as the heat flux rises; in the high vapor-quality region, the vapor-phase concentration difference, in turn, increases significantly with the increase in heat flux.

(4) The present model was confirmed by the R50/R170 experimental data. The result indicated that the predictions of new model exhibit robust consistency with experimental results with an ARD of -0.14% and a MARD of 11.47%.

5. Outlook for future investigation

This model features universality, as its theoretical framework is based on the conservation of mass and energy as well as the non-equilibrium theory, and is not dependent on specific working fluids. During the operation of the model, thermophysical parameters are retrieved in real time from NIST REFPROP. Therefore, the model can be applied to other working fluids without the need to adjust core parameters. However, several avenues remain open for further investigation to extend its applicability and accuracy.

(1) The application scope of multi-component mixtures is expanding increasingly, and they have gradually become an important development direction in refrigeration and energy systems.

Therefore, based on the existing binary mixtures, the condensation heat transfer characteristics of multi-component mixtures will be further investigated to verify the applicability of the model in more complex systems.

(2) Considering the diverse channel structures and wide range of operating conditions in engineering applications, experimental studies under different geometric cross-sections and a wider range of pressures and heat flux will be carried out in subsequent research to evaluate the predictive ability of the model under more extensive conditions.

(3) Apply this model to the design and optimization of microchannel heat exchangers, especially for improving the performance of refrigeration systems and heat pump systems using low-GWP working fluids.

Acknowledgments

This work was supported by National Natural Science Foundation of China (Grant No. 52106016), College Youth Innovation Team of Shandong Province, China (Grant No. 2024KJH151), Young Talent of Lifting Engineering for Science and Technology in Shandong, China (Grant No. SDAST2024QTA048) and Key R & D Program of Shandong Province, China (2022CXGC020901).

Nomenclature

Latin symbols	
D	inner diameter [m]
G	mass flux [kg m^{-2} s^{-1}]
h	heat transfer coefficient [W m^{-2} K^{-1}]
J	diffusion coefficient [m^{2} s^{-1}]
k	thermal conductivity [W m^{-1} K^{-1}]
m	mass condensation flux [kg m^{-2} s^{-1}]
Nu	Nusselt number
Pr	Prandtl number
Re	Reynolds number
Sc	Schmidt number
Sh	Sherwood number
T	temperature [K]
x	vapor quality
X	liquid concentration of more volatile component
Y	vapor concentration of more volatile component
z	The position of the condensation section
Greek letters	
ρ	density [kg·m^{-3}]
Subscript	
b	bulk flow
i	interfacial
l	liquid phase
t	total
v	vapor phase
w	inner-wall

References

[1] Maråk. Condensation heat transfer and pressure drop for methane and binary methane fluids in small channels. Norwegian University of Science and Technology, Trondheim 2009.
[2] Zhuang, X. R., Chen, G. F., et al. Experimental investigation on flow condensation of methane in a horizontal smooth tube. International Journal of Refrigeration. 78 (2017) 193-214.
[3] Zhuang, X. R., Chen, G. F., et al. Experimental investigation on flow condensation of zeotropic mixtures of methane/ethane in a horizontal smooth tube. International Journal of Refrigeration. 85 (2018) 120-134.
[4] Gong, M. Q., Wu, J. F., et al. Study of the single-stage mixed-gases refrigeration cycle for cooling temperature-distributed heat loads. International Journal of Thermal Sciences. 43 (2004) 31-41.
[5] Song, Q., Wang, D., et al. Experimental and analytical investigation on flow condensation heat transfer of zeotropic mixtures of tetrafluoromethane/ethane. Applied Thermal Engineering. 197 (2021) 117382.
[6] Song, Q., Wang, D., et al. Flow condensation pressure drop characteristics of zeotropic mixtures of tetrafluoromethane/ethane: Experimental and analytical investigation. International Journal of Heat and Mass Transfer. 182 (2022) 122045.
[7] Lim, W., Choi, K., et al. Current status and perspectives of liquefied natural gas (LNG) plant design. Industrial & Engineering Chemistry Research. 52 (2013) 3065-3088.
[8] Tzabar, N. Binary mixed-refrigerants for steady cooling temperatures between 80 K and 150 K with Joule–Thomson cryocoolers. Cryogenics. 64 (2014) 70-76.
[9] Wang, Y., Zhao, Y., et al. The effective refrigeration temperature zone expressed by partial molar enthalpy difference of each component in mixed-refrigerant Joule-Thomson refrigerators. Cryogenics. 128 (2022).
[10] Wang, Y., Zhao, Y., et al. Evaluation and analysis from pressure and component in the single-stage mixed-refrigerant Joule-Thomson cooler from 100 to 200 K. Energy. 319 (2025).
[11] Zou, L., Bai, T., et al. Experimental study on the characteristics of R1150/R600 mixed refrigerant Joule-Thomson low-temperature freezer. Applied Thermal Engineering. 249 (2024).
[12] Colburn, A. P., Drew, T. B. The condensation of mixed vapors. Trans AIChE. 33 (1937) 197-215.
[13] Price, B. C., Bell, K. J. Design of binary vapor condensers using the Colburn-Drew equations. AIChE Symp Ser. 70 (1974) 163-171.
[14] Jin, D. X., Kwon, J. T., et al. Prediction of in-tube condensation heat transfer characteristics of binary refrigerant mixtures. International Journal of Refrigeration. 26 (2003) 593-600.
[15] Wang, L., Jiao, P., et al. Condensation heat and mass transfer characteristics of low GWP zeotropic refrigerant mixture R1234yf/R32 inside a horizontal smooth tube: An experimental study and non-equilibrium film model development. International Journal of Thermal Sciences. 170 (2021) 107090.
[16] Wang, L., Dang, C., et al. Experimental and Theoretical Study on Condensation Heat Transfer of Nonazeotropic Refrigerant Mixtures R1234yf_R32 Inside a Horizontal Smooth Tube. International Refigeration and Air Conditioning Conference2012. (2012).
[17] Wang, L., Dang, C., et al. Study on condensation heat transfer characteristics of nonazeotropic binary refrigerant mixture R1234yfR32 inside small-scale horizontal smooth tubes. 2013 Heat Transfer Summer Conference. ASME, Minneapolis, MN, USA, 2013. pp. pp. 1-7.
[18] Deng, H., Fernandino, M., et al. Numerical study of heat and mass transfer of binary mixtures condensation in mini-channels. International Communications in Heat and Mass Transfer. 58 (2014) 45-53.
[19] Zhang, Y., Jia, L., et al. Analytical model for the condensation heat and mass transfer characteristics of binary zeotropic mixtures. International Journal of Heat and Mass Transfer. 142 (2019) 118487.
[20] Wu, Z., Xia, Y., et al. A novel condensation heat transfer correction based on non-equilibrium film theory and degradation mechanism for zeotropic mixture. International Communications in Heat and Mass Transfer. 160 (2025) 108342.
[21] Yan, S., Dong, X., et al. A new heat transfer model based on non-equilibrium film theory for annular flow condensation of binary zeotropic mixtures. International Journal of Heat and Mass Transfer. 205 (2023) 123899.
[22] Yan, S., Dong, X., et al. A new heat transfer model based on non-equilibrium theory for annular flow condensation-part II: Ternary zeotropic mixtures. International Journal of Heat and Mass Transfer. 221 (2024) 125026.
[23] Zhuang, X., Chen, G., et al. Experimental investigation on flow condensation of zeotropic mixtures of methane/ethane in a horizontal smooth tube. International Journal of Refrigeration. 85 (2018) 120-134.
[24] Lemmon, E. W., Huber, M. L., et al. NIST standard database 23, Version 9.1. Applied Chemicals and Materials Division. (2013).
[25] Koyama, S., Yu, J., et al. Condensation of binary refrigerant mixtures in a horizontal smooth tube. Thermal Science and Engineering Progress. 6 (1998) 123-129.
[26] Lamourelle, A. P., Sandall, O. C. Gas absorption into a turbulent liquid. Chemical engineering science. 27 (1972) 35-43.
[27] Poling, B. E., Prausnitz, J. M., et al. The Properties of Gases and Liquids. 5th ed. ed. McGRAW-HILL2000 (Chapter 11).
[28] Kim, C.-H., Kim, N.-H. Condensation heat transfer and pressure drop characteristics of low GWP R-404A alternative refrigerants in a multiport tube having axial microfins. International Journal of Heat and Mass Transfer. 188 (2022) 122624.
[29] Garimella, S., Milkie, J., et al. Condensation of zeotropic mixtures of low-pressure hydrocarbons and synthetic refrigerants. International Journal of Heat and Mass Transfer. 162 (2020) 120301.
[30] Mazumder, S., Afroz, H. M. M., et al. Study of in-tube condensation heat transfer of zeotropic R32/R1234ze(E) mixture refrigerants. International Journal of Heat and Mass Transfer. 169 (2021) 120859.
[31] Wang, L., Dang, C., et al. Condensation heat and mass transfer characteristics of zeotropic refrigerant mixture R1234yf/R32 inside small-scale tube: Flow patterns observation and non-equilibrium film model calculation. International Journal of Thermal Sciences. 191 (2023) 108347.

Submitted: 24.6.2025.
Revised: 21.9.2025.
Accepted: 26.9.2025.